Negative Ion Based Neutral Injector: Beam Formation and Transport

A. A. Ivanov, Yu. Belchenko, P. Deichuli, A. Sanin, O. Sotnikov [a)]

Budker Institute of Nuclear Physics, Novosibirsk, RUSSIA

[a)]Corresponding author: o.z.sotnikov@inp.nsk.su

Abstract. The essential feature of designed at Budker Institute of Nuclear Physics negative-ion-based neutral beam injector is the beam transport from the source to a single-aperture 0.5 ÷ 1 MeV accelerating tube trough a low energy beam transport line (LEBT). This scheme purifies the beam from the co-streaming fluxes of electrons, hydrogen atoms, molecules, and cesium vapor. As a result, the loading on the accelerating tube is considerably reduced. It will enable more stable operation of the accelerator. We report the first experimental results on 1.2 A, 85 keV H- beam transport through the LEBT to calorimeter.

INTRODUCTION

The construction of 5 MW negative-ion-based neutral beam injector (N-NBI) producing the neutral beam with energy up to 1 MeV is in progress at Budker Institute of Nuclear physics (BINP) [1]. The scheme used in BINP project differs from the standard versions of N-NBI injectors. The typical arrangement of experimental high energy neutral beam injectors for thermonuclear fusion comprises negative ion source directly attached to a multi-aperture accelerator. This scheme suffers from high loads of the accelerating section by the co-streaming fluxes of primarily and secondary particles, such as electrons, cesium vapor, hydrogen atoms and molecules. These high loads strongly reduce the voltage holding capacity of the accelerator. Essential feature of our scheme is that the ion source is separated from the accelerator by the LEBT [2]. In the LEBT there are two beam deflection magnets for parallel beam shift NI away from co-streaming neutrals. Also the scheme provides enough space for high-speed vacuum pumps. Thus, the loads on the accelerating tube are considerably reduced, thereby providing more stable operation of the accelerator. In the paper we report the studies on beam transport to the distant Faraday cup (FC) and to the sectioned calorimeter (SC) at the LEBT exit. The results on production and formation of 1.2 A, 85 keV beam is discussed in the accompanying paper, presented on this symposium [3].

TEST STAND DESCRIPTION

The special test stand was constructed for the study of powerful negative ion sources at BINP. Schematic top view of the stand is shown in Fig. 1. The stand consists of 3.1 m long and ∅2.1 m vacuum tank with pumping system, two separating magnets for beam parallel shift, movable Faraday cup, beam collector, and beam calorimeter, installed at place of 0.5 ÷ 1 MeV acceleration tube. Pumping system of the stand consists of two cryopumps with pumping speed up to 200 m^3/s, and a 3 m^3/s turbomolecular pump. The negative ion source with RF driver is connected to the chamber through the ∅800 mm gate valve. Main power supplies, which can provide 40 kW RF power to the plasma driver, and 120 kV/3 A acceleration power system are located at basement floor of the stand. The thermal stabilization system and other power supplies are situated at 120 kV insulated platform near the source.

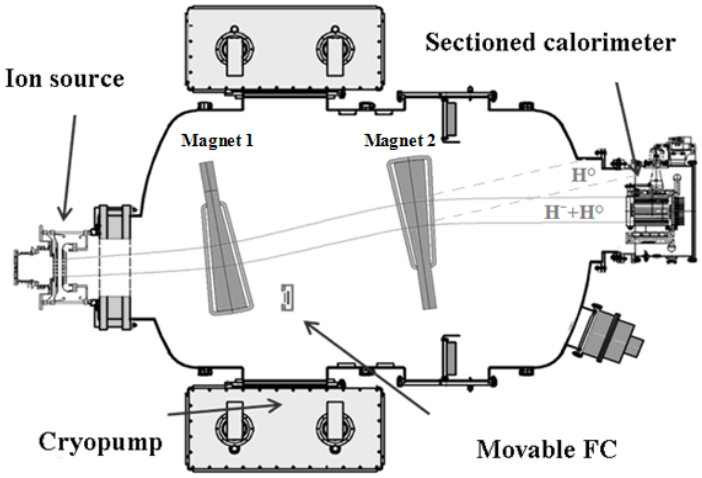

FIGURE 1. Schematic view of the BINP test stand.

The source geometry follows the traditional design of a large-area inductive radio frequency (RF) surface-plasma source of negative ions [2]. Two magnets are used for 44 cm parallel shift of the beam axis before entering the acceleration tube. The displacement of the accelerator axis protects the ion source from back-streaming positive ions, and the accelerating tube from the flux of cesium and harmful impurities, coming from the ion source side. An intense pumping by two cryopumps reduces the residual hydrogen pressure in the LEBT and decreases multiplying and avalanching of secondary particles in the accelerator.

Magnets consist of C-shaped yoke, sector-shaper poles, and 2 correction coils. Main magnetic field of 215 Gs at maximum with FWHM 240 mm for magnets #1 and 300 Gs with FWHM 200 mm for magnet #2 is produced by constant magnets. Additional coils are used to correct beam trajectory.

Three diagnostics were used to measure the current of the produced NI beam: a) the measurements of currents in the circuits of IOS power supplies [3], b) the measurements by movable FC and c) the measurements by SC.

The water-cooled FC was installed behind first magnet on the movable rod at a distance 1.6 m downstream from the source (Fig. 1), and provides the direct electrical measurements of the beam intensity and profile. The diameters of the used FC apertures (10, 100 or 170 mm) were lower, than the size of the beam, so the beam current density distribution across the beam was determined by FC scanning in the perpendicular plane. The value of total beam current was calculated by integrating the current density profile.

Beam on LEBT exit was cut by 24x24 cm^2 aperture and then the profile was measured by sectioned calorimeter at a distance 3.5 m away of the ion source grids. SC provides information of transported NI beam current and profile. In addition, the calorimeter can be used to measure current of fast neutrals born by NI stripping in drift space between deflection magnets. The calorimeter consists of 15 horizontal copper blocks cooled by water. Total height of the calorimeter is 27 cm, length – 44 cm. The temperature rise of the copper blocks was measured with brazed thermocouples. The measured by the calorimeter beam profile includes thermal effect from both negative ions and energetic neutrals, produced by stripping.

BEAM TRANSPORT THROUGH THE LEBT

The experiments on 0.7 – 1.2 A negative ion beam formation and following transport through the LEBT were carried out. The dependencies of NI beam current at IOS exit, beam current at FC plane and current, measured by calorimeter, were studied for two modifications of radio-frequency driver: with and without Faraday screen [4]. The Faraday Screen protects ceramics from erosion by the discharge plasma particles, but also decreases applied to plasma RF power. The driver without FS allows higher power RF discharge, but has limited 5 s pulse duration.

Typical distribution of beam current density, obtained by FC scan at the distance of 1.6 m from the source is shown in Fig. 2. White squares show the positions, at which the current was measured, the digits near squares - FC current at this point. Circles show areas of FC ∅ 170 mm at several positions. To calculate total beam current at FC plane, current at marked positions of FC were summarized. To consider the remaining unmeasured by FC beam current and overlapping of FC space at different positions, beam current density was interpolated. As it is seen in

Fig. 2, in the case of driver without protective FS about 90% of the beam (with energy 80 keV) has the size 33x30 cm^2.

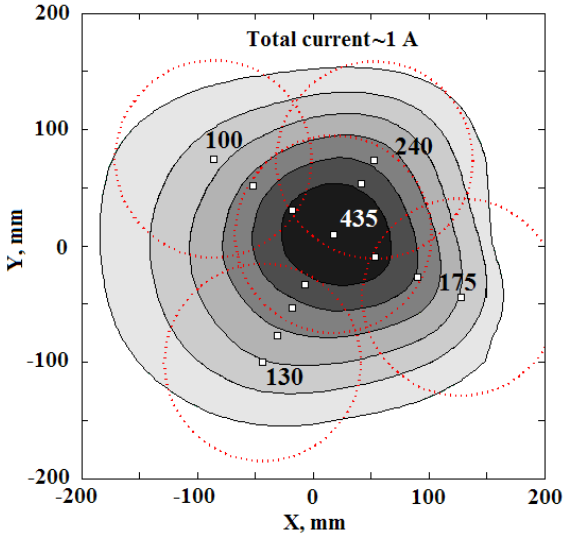

FIGURE 2. Profile of beam current, measured by movable Faraday Cup at distance 1.6 m. Squares show the FC positions at which the current was measured. Digits near squares indicate the FC current in mill Amperes. Driver without protective FS, RF power 36 kW, $U_{ex}+U_{ac}$ = 12+73 kV, P_{H2}= 0.4 Pa, I_b =1.2 A, I_C = 0.46 A, FC ∅ 170 mm.

Beam transport efficiency ratio I_{FC} / I_b to FC plane is shown in Fig. 3 vs hydrogen filling pressure at the source. Here I_{FC} is the total beam current at FC plane and I_b is the beam, outgoing from the source. RF discharge power increases with hydrogen pressure growth [2]. Line I_b in Fig. 3 shows the NI current, outgoing from the source. The I_b value is normalized to RF power of 25 kW according to dependencies, shown in paper [2]. As it seen from Fig. 3, the normalized beam current I_b decreases with pressure growth due to increased H^- ions stripping by hydrogen gas during the path through IOS. However, the efficiency of beam transport I_{FC} / I_b is about 0.9, and slightly depends on hydrogen filling pressure. It shows that the dominant stripping of H^- ion beam is produced in the area of acceleration gap and inside the grid support.

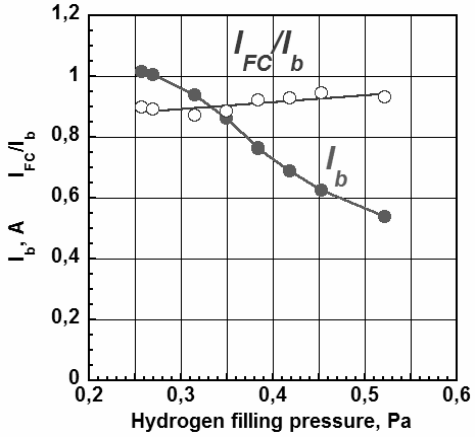

FIGURE 3. Beam transport efficiency I_{FC} / I_b and outgoing NI beam current I_b, normalized to RF power vs hydrogen filling pressure. Driver with FS. U_{ex} = 7.5 kV, U_{ac} = 67 kV, U_{PG} = 20 V.

The data on power and profiles of NI beam, transported through the LEBT to calorimeter for source modifications with and without FS in the driver is shown in Table 1. The column I_b in the table shows the NI beam current, outgoing from the source. It was I_b = 0.6 ÷ 0.8 A for the source with FS, and 1.2 A for the source without FS. The column I_{FC} shows an integral NI beam current, transported to the FC plane (at 1.6 m from the source). Column P_{SC} shows the power of main group, measured by SC (at distance 3.5 m), while column $\hat{I}_{SC}$ shows a sum of NI current with equivalent atomic current, corresponding to this P_{SC} power. Column S_{FC} shows the size of the beam, measured

at the FC plane (FWHM – see Fig. 2). Column Y_{SC} shows the vertical beam size, measured at the SC plane. The columns U_{ex}, U_{tot}, P_{RF} show the extraction voltage, NI beam energy and RF discharge power. Rows correspond to three cases: first row corresponds to typical RF power P_{RF}=25 kW with low extraction voltage U_{ex}=7 kV, second row - typical RF power with typical extraction voltage U_{ex}=10 kV, third row - increased RF power P_{RF}=36 kW with increased extraction voltage U_{ex}=12 kV. For first and third cases hydrogen filling pressure was P_{H2} = 0.4 Pa, for second case it was P_{H2} = 0.5 Pa.

Table 1. Parameters of the transported beam.

Driver	I_b, A	I_{FC}, A	P_{SC}, kW	$\hat{I}_{SC}$, A	S_{FC}, cm^2	Y_{SC}, cm	U_{ex}, kV	U_{tot}, keV	P_{RF}, kW
Driver with FS	0.6	0.5	24	0.3	17x15	16	7	80	25
Driver with FS	0.8	0.7	50	0.6	17x14	18	10	85	24
no FS	1.2	1	43	0.5	19x17	26	12	85	36

Two energetic particles groups were recorded at calorimeter plane. The main group consists mostly of NI beam, and second one consists of neutrals (marked H^0 in Fig. 1). Their profiles were identified by NI beam shift with the change of the magnetic field in the deflecting magnets. The vertical (Y) profile of the beam, entering the SC was measured by the vertical row of thermocouples installed in SC. The horizontal (X) profile of beam current density was measured by beam scanning in X direction with the magnetic field change. The data from vertical row of SC thermocouples versus the magnetic field of first magnet B_1 is shown in Fig. 4. There are two peaks in the XY profile of the beam. The intense peak at the right in Fig. 4 displays the beam main group. It mainly consists of the H- ions and partially includes the energetic neutrals, produced by stripping of NI in the drift space after the second deflection magnet. The left peak in Fig. 4 consists of neutrals, produced by NI stripping in the space between magnets #1 and #2. Beam shift along X axis was calibrated by the deflecting of beam maximum over the horizontal row of thermocouples, attached to the central calorimeter block. The top axis in Fig. 4 shows the beam shift along X-axis at SC plane, corresponding to the applied magnetic field of LEBT magnet #1.

Beam current at IOS exit I_b =0.56 A corresponds to beam power 45 kW. Beam power accepted by calorimeter of right peak is P_{SC} = 24 kW. Power of left peak P_{SC} = 4.5 kW agrees with theoretical estimation of ~10% beam striping in the region between magnets with corresponding hydrogen pressure $7.3 \cdot 10^{-3}$ Pa.

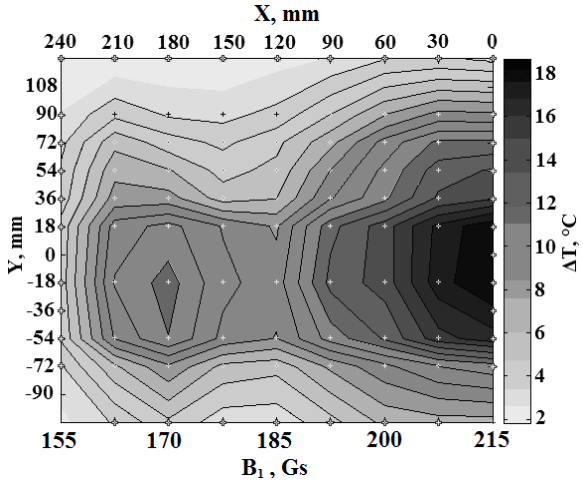

FIGURE 4. The data for the vertical row of thermocouples vs the magnetic field of the first magnet B_1. The scale (in ^{0}C) for the thermocouple temperature heating by the beam is shown at the right side. RF power 25 kW, $U_{ex}+U_{ac}$= 7+75 kV, P_{H2}= 0.4 Pa, I_b =0.56 A. Driver with FS.

The vertical profile of the beam main group was measured by the vertical row of thermocouples, and it is shown in Fig. 5 for beams with various energy and discharge power. In the case of discharge with RF power 25 kW, extraction voltage U_{ex}=7 kV, and total energy 80 keV the main group size (FWHM) is about 16 cm (squares in Fig.5), which is smaller, than the calorimeter aperture size. For typical RF power 24 kW with extraction voltage U_{ex}=10 kV and total energy 85 keV the sizes of main group increase to 22 cm (triangles in Fig. 5) and becomes larger, than the calorimeter aperture. For the 86 keV beam, produced by the discharge with RF power 36 kW and

extraction voltage U_{ex}=12 kV (circles in Fig. 5) beam FWHM size ~26 cm exceeds the aperture size, and the beam is partly measured by calorimeter.

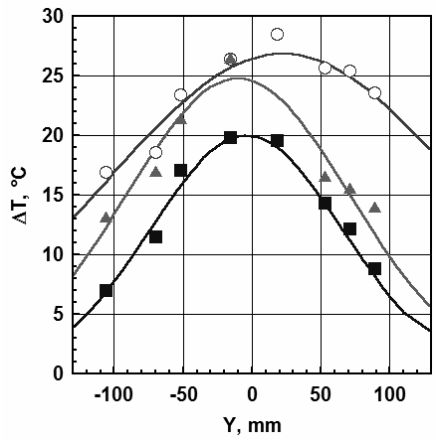

FIGURE 5. Profile of beam current, measured by sectioned calorimeter at distance 3.5 m. Markers show the temperature of various calorimeter blocks. Solid squares - driver with protective FS, RF power 25 kW, $U_{ex}+U_{ac}$= 7+73 kV, I_b=0.56 A, I_C=0.3A; Solid triangles - driver with protective FS, RF power 24 kW, $U_{ex}+U_{ac}$= 10+75 kV, I_b=0.76 A, I_C=0.55A; open circles - driver without protective FS, RF power 36 kW, $U_{ex}+U_{ac}$= 12+74 kV, I_b =1.13 A, I_C = 0.46 A

CONCLUSIONS

First experiments on beam transport through LEBT were carried out. All elements of LEBT for NI beam shifting and it's pumping system operate according to the projected parameters. In the case of initial NI beam with current I_b= 0.8 A and energy 85 keV, recorded at the source exit, about 70% of the beam was transported to the plane of distant calorimeter, located at 3.5 m from source. The full size of 86 keV beam, transported to the SC plane, was larger, than the size of the calorimeter inlet aperture. At increased acceleration voltage and optimized extraction voltage the beam divergence will be smaller, and the beam transport will improve.

ACKNOWLEDGEMENTS

This work has been supported by Russian Science Foundation (Project N 14-50-00080).

REFERENCES

[1] Yu. Belchenko, A. Gorbovsky, A. Ivanov, S Konstantinov, A. Sanin, I Shikhovtsev, M Tiunov, AIP Conf. Proc. **1515**, 167 (2013), doi: 10.1063/1.4792783

[2] Yu. Belchenko, G. Abdrashitov, P. Deichuli, A. Ivanov, A. Gorbovsky, A. Kondakov, A. Sanin, O. Sotnikov, I. Shikhovtsev, Rev. Sci. Instrum., **87**, 02B316 (2016), doi: 10.1063/1.4932583

[3] G. Abdrashitov, Yu. Belchenko, A. Ivanov, S. Konstantinov, A. Sanin, N. Stupishin, O. Sotnikov, I. Shikhovtsev, "Emission properties of Inductively Driven Negative Ion Source for NBI", AIP Conf. Proc. (these proceedings).

[4] Yu. Belchenko, A. Ivanov, A. Sanin, O. Sotnikov, I. Shikhovtsev, Rev. Sci. Instrum., **87**, 02B119 (2016), doi: 10.1063/1.4932581